A. Spinelli, F. Cozzi, G. Cammi, M. Zocca, P. Gaetani, V. Dossena, A. Guardone
Preliminary Characterization of an Expanding Flow of Siloxane Vapor Mdm
Journal of Physics: Conference Series, Vol. 821, N. 1, 2017, 012022 (10 pages)
doi:10.1088/1742-6596/821/1/012022

IOP Conf. Series: Journal of Physics: Conf. Series **821** (2017) 012022 doi:10.1088/1742-6596/821/1/012022

Preliminary characterization of an expanding flow of siloxane vapor MDM

A. Spinelli[1], F. Cozzi[1], G. Cammi[1], M. Zocca[2], P. Gaetani[1], , V. Dossena[1] and A. Guardone[1]

[1] Department of Energy, Politecnico di Milano
Via Lambruschini 4, 20156, Milano, Italy
[2] Department of Aerospace Science and Technology, Politecnico di Milano
Via La Masa 34, 20156, Milano, Italy

E-mail: andrea.spinelli@polimi.it, alberto.guardone@polimi.it

Abstract. The early experimental results on the characterization of expanding flows of siloxane vapor MDM ($C_8H_24O_2Si_3$, octamethyltrisiloxane) are presented. The measurements were performed on the Test Rig for Organic VApors (TROVA) at the CREA Laboratory of Politecnico di Milano. The TROVA test-rig was built in order to investigate the non-ideal compressible-fluid behavior of typical expanding flows occurring within organic Rankine cycles (ORC) turbine passages. The test rig implements a batch Rankine cycle where a planar converging-diverging nozzle replaces the turbine and represents a test section. Investigations related to both fields of non-ideal compressible-fluid dynamics fundamentals and turbomachinery are allowed.The nozzle can be operated with different working fluids and operating conditions aiming at measuring independently the pressure, the temperature and the velocity field and thus providing data to verify the thermo-fluid dynamic models adopted to predict the behavior of these flows. The limiting values of pressure and temperature are 50 bar and 400 °C respectively. The early measurements are performed along the nozzle axis, where an isentropic process is expected to occur. In particular, the results reported here refer to the nozzle operated in adapted conditions using the siloxane vapor MDM as working fluid in thermodynamic regions where mild to medium non-ideal compressible-fluid effects are present. Both total temperature and total pressure of the nozzle are measured upstream of the test section, while static pressure are measured along the nozzle axis. Schlieren visualizations are also carried out in order to complement the pressure measurement with information about the 2D density gradient field. The Laser Doppler Velocimetry technique is planned to be used in the future for velocity measurements. The measured flow field has also been interpreted by resorting to the quasi-one-dimensional theory and two dimensional CFD viscous calculation. In both cases state-of-the-art thermodynamic models were applied.

1. Introduction

Non-ideal compressible flows are present in a variety of industrial processes, among which energy plants based on the organic Rankine cycle (ORC) technology. Expanding flows which typically occur within ORC turbine passages are highly non-ideal and supersonic. The non-ideality is related to the proximity of the expansion processes to the critical point and to the vapor saturation curve of the working fluid, while the high Mach numbers result from the high molecular complexity and molecular mass exhibited by the organic working fluids employed in

ORC applications. Currently, no experimental data are available to characterize these non-ideal flows and to verify the accuracy of the numerical tools that are used in order to design and optimize ORC turbine blades. These are Computational Fluid Dynamic (CFD) codes implementing state-of-the-art thermodynamic models to predict the thermodynamic properties of the working fluids [1, 2, 3, 4, 5, 6]. The accuracy of these codes needs to be assessed, especially within close to saturation thermodynamic regions. Aiming at providing experimental data to improve the fundamental knowledge of non-ideal compressible flows and test cases to be compared with CFD calculations, especially for ORC applications, the *Test Rig for Organic VApors* (TROVA) has been built at the CREA Laboratory of Politecnico di Milano [7]. Expanding flows of different organic compounds in non-ideal conditions can be investigated within the TROVA by independent measurements of pressure, temperature and velocity. The facility implements a batch organic Rankine cycle (either sub-critical or super-critical), where the expansion process take place within a nozzle replacing the turbine. A straight axis, planar converging-diverging nozzle has been selected as the test section, being suitable to perform experiments of significance for both non-ideal gas-dynamics fundamentals and ORC turbine flows. The nozzle size (20 mm is the equivalent diameter at the geometrical throat) is large enough to preserve a large isentropic core of the expanding flow, therefore the temperature and pressure fields can be gathered without the use of calibrated probes, see [8]. Total pressure and temperature are measured in the settling chamber ahead of the nozzle inlet; static pressure taps at different sections along the nozzle axis are used to follow the flow evolution as it expands from rest to supersonic conditions.

The paper reports the early experimental observation of the expanding flow of siloxane MDM vapor at mild and medium non-ideal conditions. Section 2, presents the general set-up of the test-rig and an overview of the measurement techniques adopted. Within section 3, experimental results for siloxane vapor MDM ($C_8H_{24}O_2Si_3$, octamethyltrisiloxane) are reported in terms of pressure and temperature measurements and of Schlieren visualization. Experimental data have been also compared with two-dimensional viscous flow calculation. Final remarks and observations are reported in section 4.

2. TROVA: set-up and measurement techniques

The TROVA operates as a blow-down wind tunnel, namely, in a discontinuous way, to reduce the power requirements. The fluid under test is stored in a high pressure vessel (HPV) (see figure 1) and isochorically heated up to saturated, superheated, or supercritical conditions (point 4 in figure 1) at a pressure P_4 and temperature T_4 above the nozzle stagnation conditions (point 6). The heating system consist of electrical bands and wires assembled on the external surface of the HPV and of the high pressure pipeline (up to valve V4, see 1). A fast operating control valve (MCV) regulates the flow rate, thus the total pressure P_{T6} at the inlet of the nozzle during the entire test. The vapor is then expanded (to state 7) through the nozzle, where wall pressure measurements are performed. The vapor is discharged into a large area pipe (point 8) and then brought in a low pressure vessel (LPV, state 9) where the fluid is condensed (state 1). The loop is closed by the liquid compression to the HPV (point 2), performed by a membrane pump. Further details on the test rig design and arrangement are in [7].

Within the TROVA test section, the expansion flow of different organic vapors can be investigated at different operating conditions, providing that a proper nozzle profile is designed for each test [9]. The initial test scheduled concern the expansion flow of siloxane MDM, a fluid is of particular interest for industrial ORC plant exploiting relatively high temperature sources (e.g. biomass, solar radiation). The operating conditions of interest for current and future tests are summarized in table 1, as computed using the Span-Wagner thermodynamic model of MDM (see [10]) implemented in FluidProp [11]. Test labeled as MDM_{SC} and MDM_{SH} are the TROVA design cases, here reported for completeness; they allow to investigate, respectively,

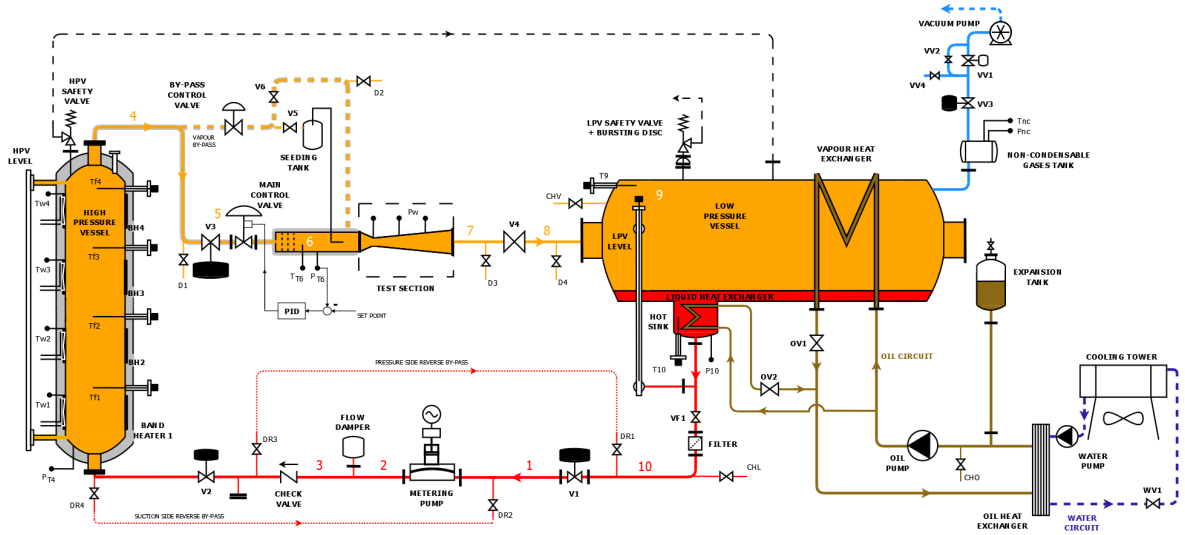

Figure 1: Scheme of the TROVA test-rig. The total conditions in the settling chamber are measured by sensors P_{T6} and T_{T6}, respectively. Static pressure taps in the test section are indicated by P_w.

Siloxane fluid MDM ($C_8H_{24}O_2Si_3$, octamethyltrisiloxane)					
TEST	P_{T6} [bar]	T_{T6} [°C]	Z_{T6}	β	M_7
MDM_0	3.15	246.0	0.88	10.08	2.12
MDM_1	4.57	245.7	0.82	9.80	2.10
MDM_2	4.40	240.4	0.82	9.81	2.10
MDM_{SH}	*25.0*	*310.3*	*0.31*	*25.0*	*2.25*
MDM_{SC}	*10.0*	*276.9*	*0.62*	*10.0*	*2.05*

Table 1: Operating conditions for the early test performed MDM_0, MDM_1, MDM_2 and for the TROVA design cases MDM_{SH}, MDM_{SC}. The expansion ratio β and exit Mach number M_7 refer to adapted conditions.

flows representative of supercritical and subcritical ORC turbine expansions. In both cases strong non-ideal effects are expected, as indicated by the value of the compressibility factor $Z = Pv/RT$, which is unity for ideal gas conditions. Three tests are reported in this paper, labeled as MDM_0, MDM_1 and MDM_2. The initial conditions of test MDM_0 correspond to mild non-ideal gas state, while the staring thermodynamics points of tests MDM_1 and MDM_2 are in medium non-ideal conditions. All test have been designed in order to reach moderate maximum values of temperatures (to avoid the risk of fluid decomposition) keeping at the same time appreciable non-ideal effects. The expansion processes described are reported in the temperature-specific entropy diagram ($T - s$) for MDM (see figure 2) referring to the initial time of each test.

2.1. Test section and instrumentation

The test section consist of a planar converging-diverging nozzle (see figure 3); the diverging portion of the nozzle profile was designed by applying the method of characteristics coupled with state-of-the-art thermodynamic models for the siloxane MDM ([9],[10]), while the converging

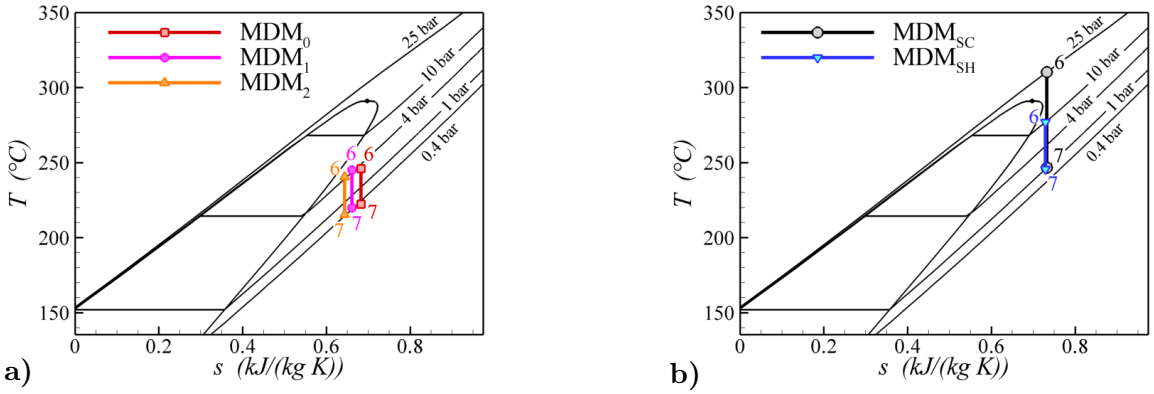

Figure 2: Overview of the expansion processes of interest for the MDM vapor. *a)* Actual expansion performed in the early tests. *b)* TROVA design expansion processes.

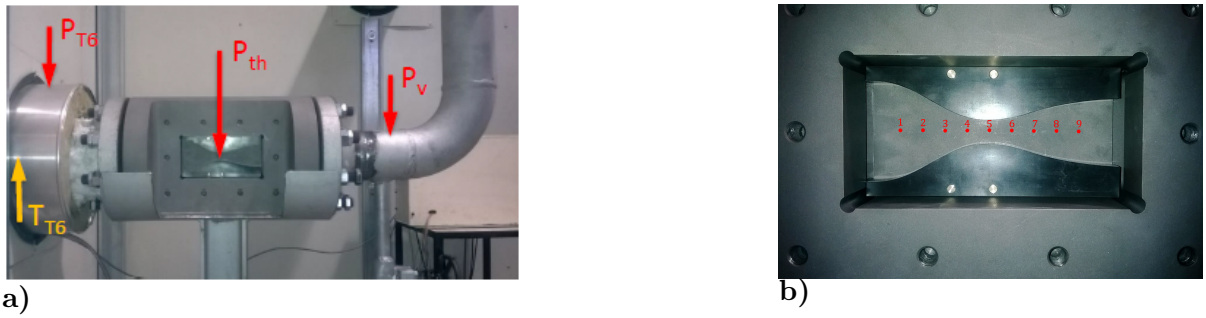

Figure 3: Overview of the test section (a) and details of the nozzle (b). The flow is from left to right. The settling chamber is on the left. The front window allows for optical access, the back closure is mirror polished (not installed to take the picture). Static pressure taps are located along the symmetry axis and are marked with red dots. The measuring point for total conditions (P_T6, T_T6) and for the downstream static pressure (P_v) are also indicated.

portion was realized was using a 5^{th} order polynomial profile At the geometrical throat a recessed step of 0.1 mm depth (1.2% of the nozzle semi-height at the throat) was machined on the contoured profiles in order to fix the location of the minimum nozzle area, independently from possible boundary layer unsteadiness.

The frontal optical access is guaranteed by a planar quartz window, while 9 pressure taps along the nozzle axis are machined on the rear steel plate. Each tap is connected with the sensing element, a piezo-resistive pressure transducer, via a 25 mm long pneumatic line-cavity system exhibiting a 0.3 to 1.5 mm diameter. The volume of the capacities ahead of the transducer sensor is extremely small ($\sim 45\ mm^3$). A natural frequency of about 900 Hz has been estimated for the transmission lines by applying a viscous model developed for an arbitrary complex system of lines and cavities [12]; the non-ideal behavior of the flow has been here neglected.

In order to perform Schlieren visualization in a double passage configuration (see 2.2), the plate surface has been mirror polished. The stagnation conditions are measured in the settling chamber ahead of the test section. A wall pressure tap/line/transducer system is used also for the total pressure, due to the very low flow velocity in the chamber; the total temperature is measured by a K type thermocouple whose hot junction is located at the chamber axis.

All pressure sensors are piezo-resistive transducers (Kulite XTEH-7L series) operating at high temperature (up to 343 °C). The data acquisition (DAQ) system consist of analog modules for

Property	**Sensor**	**Type**	**CR *P*** (**bar**)	**CR *T*** (**C**)	**U$_2$ *P*** (**%FS**)	**U$_2$ *T*** (**C**)
T_T	Thermocouple	K (Ni/Cr - Ni/Al)	-	25-300	-	1.0
P_T, P_w	Piezo-resistive	Kulite XTEH	1-FS (3.5-40)	25-300	~ 0.07	-

Table 2: Type, calibration range (CR) and expanded uncertainty (U_2) of the instruments employed for pressure and temperature measurements. FS is the transducer full scale.

signal conditioning and of a high speed 16 bit ADC data acquisition board. The K thermocouple has been calibrated in the temperature range 25-300 °C . Due to the large sensitivity of the pressure transducers to temperature variation they were calibrated both in pressure and in temperature in the range of 1 bar to full scale for the pressure and of 25-300 °C for the temperature. The final accuracy of each sensor is summarized in table 2.

2.2. Schlieren set-up

The adopted Schlieren system is of double passage type, with the emitting and receiving optical components on the same optical bench. This solution entails the indubitable advantage of easy alignmentThe light emitted from a 100 W Hg arc-lamp is focused by a F/1.5 silica lens and then collimated by a Schlieren lens head of 150 mm diameter and 1000 mm. The parallel light rays traverse the test section and are then reflected back to the Schlieren head by the polished nozzle back wall (where also the pressure taps are located) and focused on the knife edge The knife orientation is vertical, thus allowing to visualize the density gradient along the horizontal nozzle axis. A semi-reflecting prism split the light beam originated by the light source and the reflected one. Finally, a real image of the test section is formed on the sensor of a high speed CMOS camera, focused by a lens of 75 mm focal lenght and 50 mm diameter) located behind the knife. The CMOS camera resolution and frame rate were respectively set to 1936 x 1216 pixels and to 20 fps (frames per second), while the exposure time was set to 1 ms. For further details on the Schlieren bench refer to [13].

3. Non-ideal nozzle flows of MDM vapor

Results from test MDM_0 (see table 1) are here reported in detail and then compared with the results of tests MDM_1 and MDM_2. Each test is triggered by the opening of the valve V3 (figure 1). The main control valve MCV has been set at a fixed position corresponding to 100% opening, in order to leave the total conditions P_{T6}, T_{T6} varying according to the HPV emptying and, therefore, exploring a wider range of inlet thermodynamic conditions and, possibly, of intensity of non-ideal behavior.

The measured test conditions in the settling chamber at time $t = 0$ s, are reported in table 1. Time $t = 0$ s has been selected at the conclusion of the initial transient. The measured value of the pressure P_{T6} and temperature T_{T6} are used to compute the value of the compressibility factor Z_{T6} and of the fundamental derivative of gasdynamics Γ_{T6} from the thermodynamic model [10]. These quantities are assumed to be the total ones, due to the very low flow velocity in the settling chamber (around 1 m/s). From time $t = 0$ s to time $t = 33$ s the nozzle operated in supersonic adapted conditions. This time interval is considered as the reference test duration for the data analysis. For the three cases, the explored regions in terms of stagnation conditions is represented in Figure 4 a) in the temperature-entropy plane.The entropy is computed from the thermodynamic model using the measured values of the total pressure and temperature.

All the investigated expansion processes are found to occur in non-ideal compressible-fluid region, as it is shown by the computed value of compressibility factor Z and of fundamental

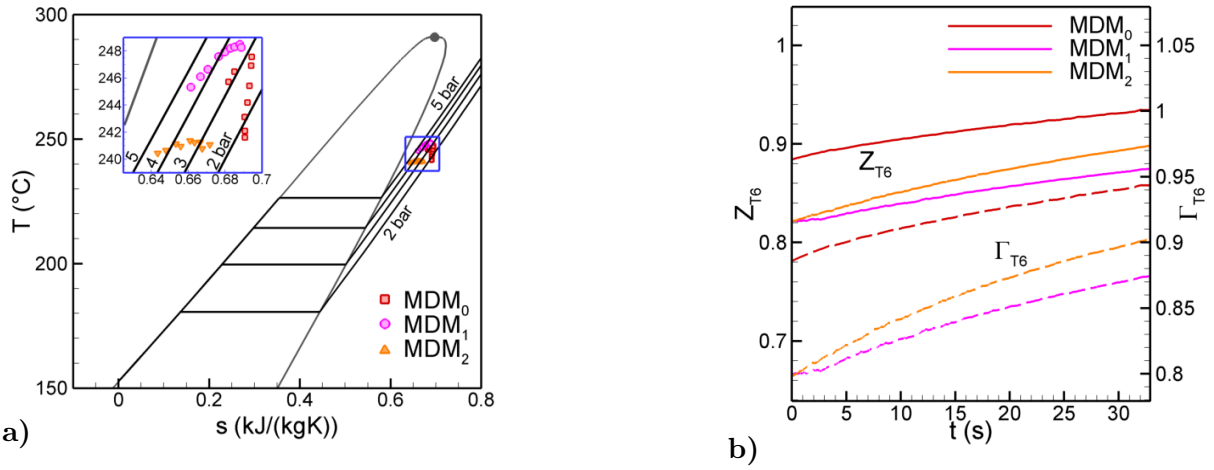

Figure 4: *a)* Thermodynamic states in the settling chamber during each test run. The entropy is computed from the thermodynamic model using the measured values of the total pressure and temperature. *b)* Computed values of the compressibility factor Z and of the fundamental derivative of gasdynamics in the settling chamber.

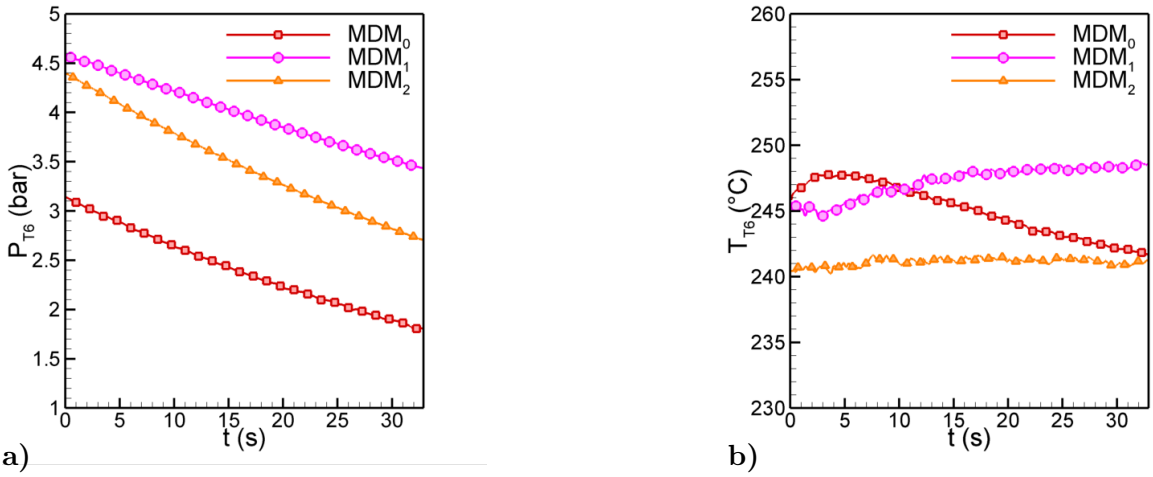

Figure 5: Measured total condition at the nozzle inlet of the three test as a function of time from $t = 0$ s and $t = 33$s. *a)* Total pressure P_{T6}. *b)* Total temperature T_{T6}.

derivative of gasdynamics Γ in the settling chamber (subscript $T6$); see figure 4 b). Mild non-ideal conditions characterize the MDM_0 expansion, while medium non-ideal states are explored during MDM_1 and MDM_2 tests.

Figure 5 shows the measured total pressure P_{T6} and temperature T_{T6} as a function of time from $t = 0$ s and $t = 33$s for the presented tests. The total pressure always decreases because the control valve is left fully open during the test run and the HPV empties. Correspondingly, the static pressure at the geometrical throat (not shown in the picture) is found to decrease with time. On the other hand the total temperature T_{T6} exhibits a non-monotonic trend, which is reasonably related to a non-uniform temperature distribution within the HPV and the downstream pipeline (up to valve V_3, see figure 1). In the following, a detailed discussion of

t [s]	P_{T6}/P_v	P_{T6} [bar]	T_{T6} [C]	Z_{T6}	γ_{T6}	Γ_{T6}	P_{th} [bar]	Z_{th}	γ_{th}	Γ_{th}	$Re_{x,th}$
0.0	6.0	3.146	245.7	0.88	1.033	0.89	2.027	0.93	1.027	0.93	1.22×10^7
9.5	5.6	2.666	246.9	0.90	1.030	0.91	1.710	0.94	1.025	0.95	1.02×10^7
20.5	5.5	2.203	244.2	0.92	1.027	0.93	1.415	0.95	1.024	0.96	8.48×10^6
30.4	5.5	1.885	242.1	0.93	1.026	0.94	1.192	0.96	1.023	0.97	7.29×10^6

Table 3: Measured stagnation conditions (subscript $T6$) and throat conditions (subscript th) for the MDM_0 test. P_{T6}/P_v represents the nozzle expansion ratio. The values of the compressibility factor Z, of the specific heat ratio γ, of the fundamental derivative of gasdynamics Γ, and of the Reynolds number $Re_{x,th}$ (based on the nozzle axial distance at the throat) are estimated from the thermodynamic and transport property models [10].

the results obtained for the MDM_0 is presented. Results of tests MDM_1 and MDM_2 are finally presented by comparison with those obtained for MDM_0.

Table 3 reports relevant flow quantities at four different time levels, namely, for $t = 0.0$ s, $t = 9.5$ s, $t = 20.5$ s and $t = 30.4$ s. The ratio of the total pressure P_{T6} to the downstream pressure P_v is such that the nozzle is choked for the entire test. At the geometrical throat, the model input are the measured static pressure and the stagnation entropy, which is assumed to be constant during the expansion (isentropic expansion along the nozzle axis) and it is therefore computed from P_{T6} and T_{T6}. The computed compressibility factors, at both the settling chamber and the geometrical throat, are increasing with time, as expected, since the HPV is emptying towards dilute conditions. At both locations, the calculatedf Z and Γ, confirm that the flow start in mild non-ideal conditions and then approaches more dilute states.

The pictures in figure 6 are the Schlieren visualizations at the four time levels listed in table 3. Notice that, due to a thermal dilation of the nozzle gaskets, the nozzle profile is not accurately visible in the images; therefore, a detailed picture of the visualized flow field at the geometrical throat at time $t = 0$ s is reported (Figure 6 e)). The actual nozzle profile (orange line) is overlapped to the dilated gasket profiles; the singular points (A, B and C) which define the shape of the recessed step, are also highlighted. The knife edge in the Schlieren bench is aligned in such a way that compressions appear as darker regions and expansions are associated to lighter regions. As observed already in preliminary experiments using air in dilute conditions [13], the presence of the recessed step (0.1 mm height) results in the occurrence of a complex wave system that is clearly visible in the divergent, supersonic portion of the nozzle. In particular, an expansion wave originates at the step edge (point A of Figure 6 e)) and it is immediately followed by a compression shock from the flow reattachment point (downstream point B). A second rarefaction fan is visible at the end of the recessed portion of the nozzle (point C), where a discontinuity in the surface geometry occurs.

In the first two frames in figure 6, the two expansions in the vicinity of the nozzle throat appear as dark regions, possibly due to the large offset of the light beam with respect to the receiving optics. A similar limitation of the adopted Schlieren technique was already observed for dilute air [13] close to the step edge. Indeed, the displacement of the light beam depends on the density gradient, which is larger in the vicinity of the step edge, where the density difference across the rarefaction wave occurs along a shorter flow path. The flow conditions in figures 6a) and 6b) are non-ideal and the fluid compressibility is almost one order of magnitude larger than in the ideal case of air and such are the density gradients. Therefore, the occurrence of the observed dark regions which extend further towards the axis of the nozzle is compatible with the fluid non-ideality. In figures 6c) and 6d), which correspond to fluid states closer to ideal conditions, the Schlieren image correctly represents the expansion regions as light grey

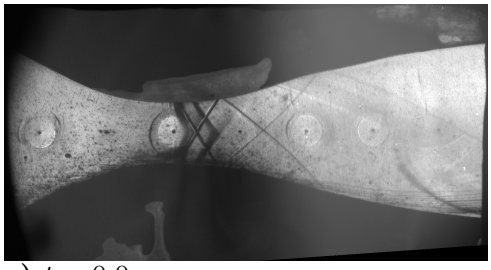

a) $t = 0.0$ s

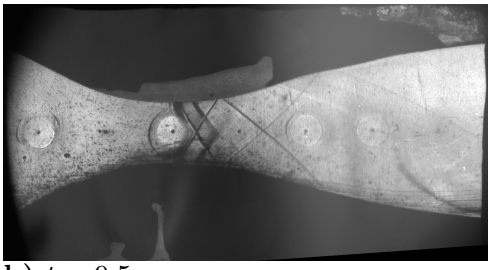

b) $t = 9.5$ s

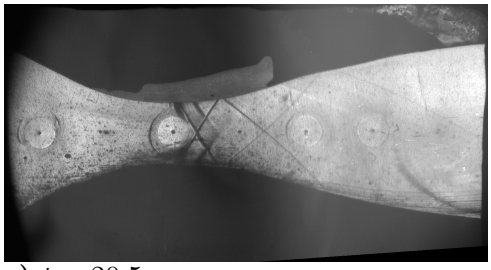

c) $t = 20.5$ s

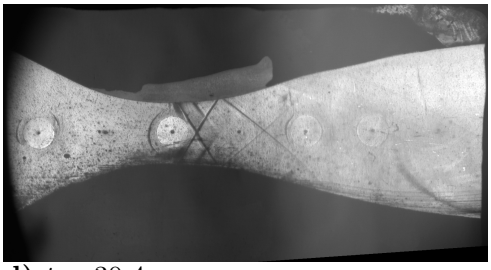

d) $t = 30.4$ s

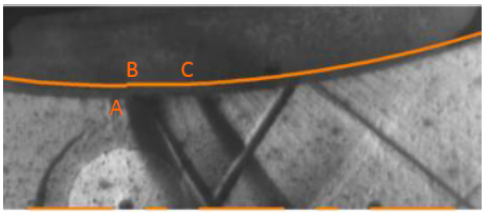

e) $t = 0.0$ s

Figure 6: Schlieren visualization of the flow field at time $t = 0.0$ s *(a)*, $t = 9.5$ s *(b)*, $t = 20.5$ s *(c)* and $t = 30.4$ s *(d)*. *(e)* Detailed view of the flow field at time $t = 0$ s. The actual nozzle profile is superimposed to the gasket profiles thermally dilated. The line segments A, B and C define the recessed step geometry.

regions and the size and shape of the dark regions closely resemble those observed in ideal gas experiments with air.

Figure 7 a) reports the comparison between the MDM run and a test with air in dilute conditions in terms of the ratio of the static pressure P_{th} at the geometrical nozzle throat to the total pressure P_{T6} from $t = 0$ s and $t = 33$s. For air in dilute conditions, the ratio is found to be constant in time, in accordance with well known results for adapted nozzles operated with ideal gases. On the contrary, for the non-ideal run with MDM, the ratio P_{th}/P_{T6} is predicted to decrease as more dilute conditions are approached. For the test MDM_0, though the nozzle is clearly working in adapted conditions in the considered time interval, this non-ideal effect is not clearly visible, since the small expected decrease (related to the mild non-ideal conditions explored) cannot be detected due to the transducer uncertainty. Therefore, in order to catch this effect, test MDM_1 and MDM_2 have been performed in higher non-ideal conditions and by using lower full scale transducers, with consequent smaller uncertainty.The trend exhibited by the P_{th}/P_{T6} ratio is now clearly decreasing as predicted by non-ideal thermodynamic models. Moreover, by comparing the P_{th}/P_{T6} trend of the three test, it can be seen that higher values are obtained in thermodynamic regions exhibiting higher non-ideal effect, namely smaller Z and Γ (see figure 4 b)), also in accordance with model predictions.

Finally the measured values of P_{th}/P_{T6} at $t = 0$ are compared with the one obtained with both inviscid and viscous CFD calculation, performed at the boundary conditions of each test at time

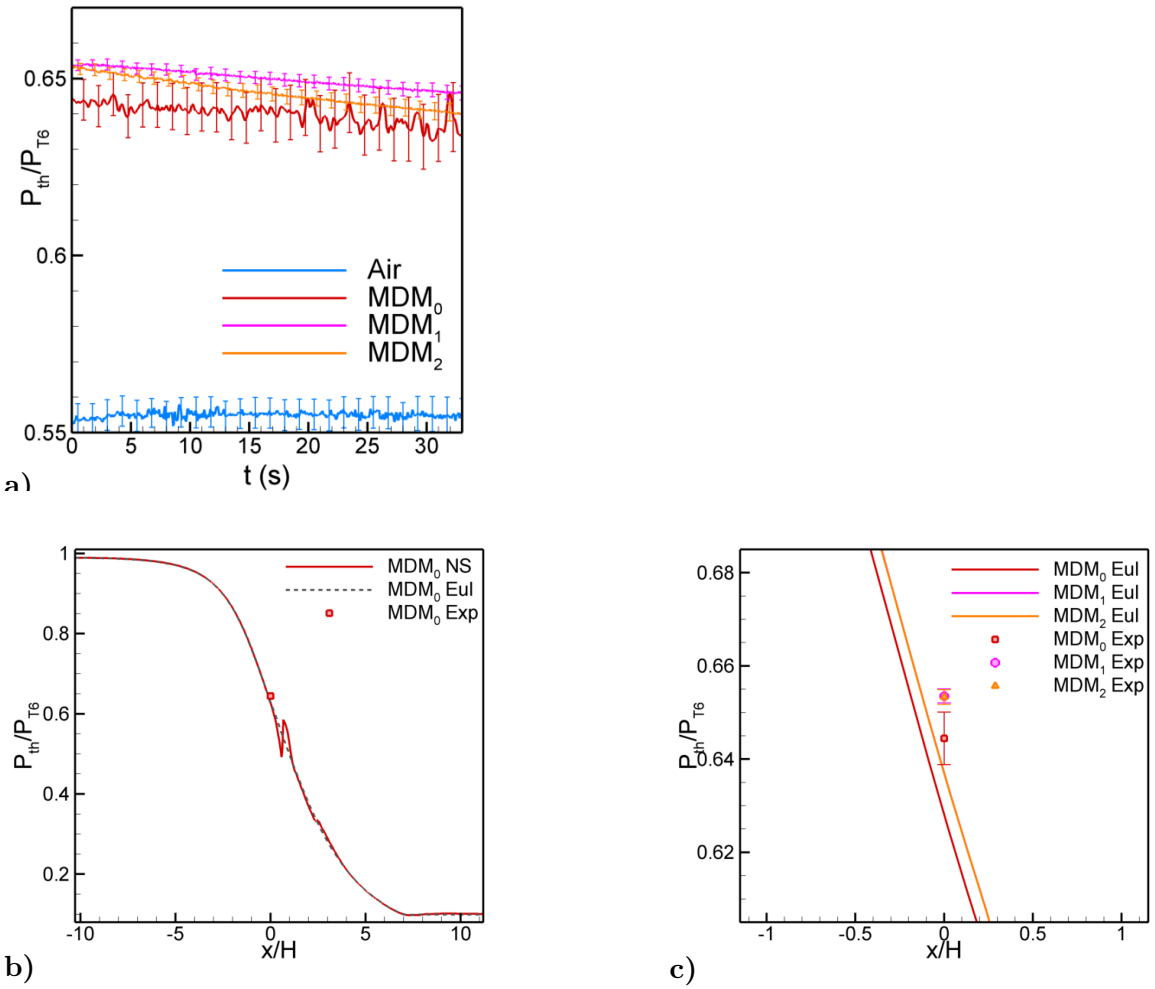

Figure 7: *a)* Static-to-total pressure ratio P_{th}/P_{T6} at the geometrical throat from $t = 0$ s and $t = 33$s for all MDM test run and for air in dilute conditions. Uncertainty bars are also reported. *b)* Comparison between experimental data (Exp) and CFD results at the nozzle axis line for the MDM_0 run at time $t = 0$. x represents the nozzle axial coordinate, H the nozzle semi-height at the throat. Inviscid (Eul) and viscous (NS) calculation have been performed, giving the same results at the throat. *c)* Detail of the comparison between experimental data and CFD inviscid calculation at the geometrical throat for the three MDM test run at time $t = 0$. MDM_1 and MDM_2 CFD plots are overlapped since the two expansion occur in the same non-ideal conditions

$t = 0$. In figure 7 b) for MDM_0 test, the experimental value (labeled Exp) of P_{th}/P_{T6} is compared with the one extracted along the nozzle axis from two two-dimensional CFD steady calculation; one inviscid (labeled Eul) and one viscous (labeled NS). In both cases, the thermodynamic model is PRSV (Peng Robinson Stryjek Vera), while the viscous calculation adopts the (k-ω SST) turbulence model implemented in the SU2 solver. The comparison shows that the inviscid calculation is able to catch the static-to-total pressure ratio up to $x/H = 0.6$, where the shock departing from the re-attachment point downstream of the step intersects the nozzle axis. For this reason in figure 7 c) the experimental values of P_{th}/P_{T6} (together with their respective uncertainty bands) obtained for the three tests are compared with the results of the inviscid calculation. The agreement between the experimental and the numerical results is very good,

being the difference of about 2.8% of the measured values for test MDM_0 and of about 2.5% for tests MDM_1 and MDM_2. This differences are probably due to a slight inaccuracy in the modeling of the boundary layer.

4. Conclusions

Preliminary results from the Test-Rig for Organic Vapors (TROVA) at Politecnico di Milano were reported here for siloxane fluid MDM ($C_8H_{24}O_2Si_3$, octamethyltrisiloxane). A subsonic-to-supersonic expansion in a converging-diverging nozzle was observed during the experimental runs. A double-passage Schlieren technique was used to visualize the streamwise density gradient and to locate the salient wave structures in the supersonic flow region. Total pressure and temperature were measured in the settling chamber. Static pressure measurement were also carried out along the nozzle axis.

The observation of shock waves induced by the recessed step confirms the occurrence of a supersonic nozzle flow of MDM in the vapor phase. The static-to-total pressure ratio measured at the geometrical throat is in accordance with values predicted by resorting to the theory of non-ideal compressible-fluid flows. Further measurement campaign are foreseen in order to complete the MDM flow characterization, they include static pressure and direct velocity measurements along the entire nozzle axis. Such experimental results can represent a useful database to verify CFD codes for non-ideal compressible flow.

References

[1] Colonna, P., and Rebay, S., 2004. "Numerical simulation of dense gas flows on unstructured grids with an implicit high resolution upwind Euler solver". *Int. J. Numer. Meth. Fluids,* ***46***(7), pp. 735–765.
[2] Guardone, A., 2007. "Three-dimensional shock tube flows of dense gases". *J. Fluid Mech.,* ***583***, pp. 423–442.
[3] Cinnella, P., and Congedo, P. M., 2007. "Inviscid and viscous aerodynamics of dense gases". *J. Fluid Mech.,* ***580***, pp. 179–217.
[4] Colonna, P., Harinck, J., Rebay, S., and Guardone, A., 2008. "Real-gas effects in organic rankine cycle turbine nozzles". *J. Prop. Power,* ***24***, March-April, pp. 282–294.
[5] Hoffren, J., Talonpoika, T., Larjola, J., and Siikonen, T., 2002. "Numerical simulation of real-gas flow in a supersonic turbine nozzle ring". *J. Eng. Gas Turbine Power,* ***124***, pp. 395–403.
[6] Pini, M., Spinelli, A., Persico, G., and Rebay, S., 2015. "Consistent look-up table interpolation method for real-gas flow simulations". *Computers and Fluids,* ***107***, pp. 178–188.
[7] Spinelli, A., Pini, M., Dossena, V., Gaetani, P., and Casella, F., 2013. "Design, simulation, and construction of a test rig for organic vapours". *ASME Journal of Engineering for Gas Turbines and Power,* ***135***, p. 042303.
[8] Spinelli, A., Dossena, V., Gaetani, P., Osnaghi, C., and Colombo, D., 2010. "Design of a test rig for organic vapours". In Proceedings of ASME Turbo Expo, Glasgow, UK.
[9] Guardone, A., Spinelli, A., and Dossena, V., 2013. "Influence of molecular complexity on nozzle design for an organic vapor wind tunnel". *ASME Journal of Engineering for Gas Turbines and Power,* ***135***, p. 042307.
[10] Colonna, P., Nannan, R., Guardone, A., and Lemmon, E. W., 2006. "Multi-parameter equations of state for selected siloxanes". *Fluid Phase Equilib.,* ***244***, pp. 193–211.
[11] Colonna, P., and van der Stelt, T. P., 2004. FluidProp: a program for the estimation of thermo physical properties of fluids. software.
[12] Antonini, C., Persico, G., and Rowe, A. L., October 13, 2008. "Prediction of the dynamic respinde of complex transmission line system for unsteady pressure measurament". *Measurament Science and Technology,* ***19***(12).
[13] Cozzi, F., Spinelli, A., Carmine, M., Cheli, R., Zocca, M., and Guardone, A., 2015. "Evidence of complex flow structures in a converging-diverging nozzle caused by a recessed step at the nozzle throat". In 45$^{\text{th}}$ AIAA Fluid Dynamics Conference, Dallas, TX, USA, 22-26 June.

Acknowledgment

The research is funded by the European Research Council under ERC Consolidator Grant 2013, project NSHOCK 617603. The initial layout of the plant was funded by Turboden S.r.l..